



Article

Impact Testing and Modelling of Composite Laminate Panels for Use in Off-Road Racing Vehicle Belly Guards

Tim Brinkmann¹ and Christiaan R. Bester^{2,*}

¹ Mechanical Engineering, University of Johannesburg, Auckland Park 2006, South Africa; timb94@gmail.com

² Department of Mechanical Engineering Science, University of Johannesburg, Auckland Park 2006, South Africa

* Correspondence: crbester@uj.ac.za

Abstract: Off-road racing vehicles require protection on the underside of their chassis in order to protect vital components from impact damage. The use of composites in thin laminate form to achieve this protection is widespread, although failure due to impact from foreign objects still occurs. The use of UHMWPE (Ultra High-Molecular Weight Polyethylene) fibres, which have superior mechanical properties to aramid fibres in vehicle belly guards, is not prevalent and, hence, could prove useful in this application. A comprehensive Finite Element Analysis (FEA) is performed in order to determine suitable laminate panel layups that can be tested, analysed, and compared to the original laminate layup, which comprises six layers of aramid and two layers of carbon fibre fabrics. This provides initial insight into the comparison of the new proposed laminates and reveals if improvements have been made. The laminates found using FEA are manufactured into panels that represent the fixture and loading cases seen in racing vehicles. Experimental testing is carried out on the various panels, and the results are compared to those of the mathematical modelling. Substituting the currently used carbon fibres with more aramid fibres increases the impact resistance of the panel. Using UHMWPE fibres greatly increases the impact resistance of the panel; however, fibre delamination becomes more prevalent. This is due to the poor fibre wettability of UHMWPE fibres and the large strain before failure of the fibres. The modelled results show good agreement with the experimental results in terms of the locations at which damage occurred.



Citation: Brinkmann, T.; Bester, C.R. Impact Testing and Modelling of Composite Laminate Panels for Use in Off-Road Racing Vehicle Belly Guards. *J. Compos. Sci.* **2023**, *7*, 440. <https://doi.org/10.3390/jcs7100440>

Academic Editor: Francesco Tornabene

Received: 27 July 2023

Revised: 30 September 2023

Accepted: 8 October 2023

Published: 17 October 2023



Copyright: © 2023 by the authors. Licensee MDPI, Basel, Switzerland. This article is an open access article distributed under the terms and conditions of the Creative Commons Attribution (CC BY) license (<https://creativecommons.org/licenses/by/4.0/>).

Keywords: composites; Dyneema; impact resistance; laminates

1. Introduction

Pure aramid-based fibre composites, such as DuPont Kevlar, have proved incapable of preventing off-road vehicle belly guards from being punctured and damaged during racing events. Figure 1 depicts damage to a belly guard. A belly guard's main purpose is to prevent rocks or foreign objects from puncturing it and potentially causing damage to the vehicle's components. Alternative materials and different composite layups need to be investigated that would improve the impact resistance of the guard while still maintaining or reducing the overall weight of the belly guard.

Many different types of materials exist that can absorb and resist impact forces in varying ways. Metallic materials can absorb a large quota of impact energy through plastic deformation mechanisms, whilst composite laminates dissipate a significant portion of energy by fracture modes, which are peculiar to this class of material. These fracture modes include matrix cracks, interlaminar delamination, fibre fracture, and fibre/matrix debonding, as described in Aymerich et al. [1]. Figure 2 shows that composite materials are able to absorb more energy on a per unit mass basis in comparison to more commonly used metals, such as steel and aluminium. Hence, composites offer the potential to be more effective in impact protection of structures. Note that the first C-FRP in Figure 2 refers mainly to an elastomer matrix material. Aymerich et al. [2] proposed numerous techniques,

ranging from the use of tough resins or high-strain fibres to the optimization of the fibre architecture to improve the impact damage resistance and tolerance of composite laminates.



Figure 1. Damage to belly guard.

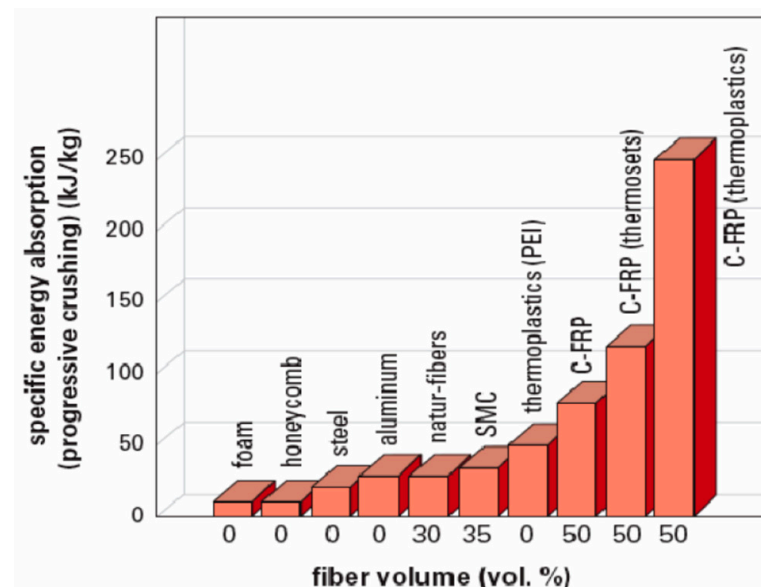


Figure 2. Specific energy absorption for various materials [3].

Composites made from carbon fibres are generally extremely strong and stiff in the fibre direction. However, carbon composite laminates are weak in the out-of-plane or transverse direction to the fibre orientation and, hence, are susceptible to failure from loads applied in these directions. Bouwmeester et al. [4] described hybridizing or laminating these composite materials with polymer fibres like aramid fibres or gel-spun polyethylene fibres to improve the resistance against impact. Attwood et al. [5] described the use of Aramid fibres, such as Kevlar, and polymer-based fibres made from ultra-high molecular weight polyethylene (UHMWPE) as the main types of fibre being used for, for example, ballistic protection due to their superior impact resistance. However, the use of UHMWPE fibres is still not as prevalent as aramid fibres due to their fairly recent introduction into the composites field. As such, the use of UHMWPE is still untested in many aspects of composite design and manufacture.

Currently, many studies of UHMWPE are not applicable to real-world situations as many of the experimental impact resistance tests are performed on samples such as 'Charpy specimens' that do not represent realistic loading situations for actual composite laminates [4].

Analysis of the low-speed impact on composites is performed in this investigation, which involves modelling the motion of an impactor, the dynamics of the structure, and the local indentation of the structure by the impactor. Abrate [6] provides a similar insight into the boundary conditions that can be expected, as well as the most appropriate model selection.

The main research objective is to determine the outcome of using UHMWPE, commonly known by the brand name DSM Dyneema, fibres in the layup sequence of the laminate for the belly guard, with the ultimate aim of preventing the guard from being punctured during competitive events.

A. Fibre and Matrix Material Overview

Composite materials are the combination of two or more materials in such a way that certain improved or desired properties are achieved, as described by Balasubramanian [7]. Harris [8] states that the materials or elements of which a composite is made work together to produce a material property that is different to the properties of the original materials on their own. Composites are mainly composed of two phases, the matrix and the dispersed phase; the matrix is also known as the bulk phase, and it is continuous and surrounds the dispersed phase. The matrix performs several critical functions, including maintaining the fibres in the proper orientation and spacing and protecting them from abrasion and the environment. The matrix transmits loads from the matrix to the fibres through shear loading at the interface, as described by Campbell [9].

Epoxy resin as a matrix has a substantially higher tensile strength as well as a higher tensile modulus than the other types of resin. Hence, its use in this case is preferred.

The dispersed phase, in this case, is the fibres that are used in composites in order to strengthen the matrix phase.

The three main fibre types are glass-, aramid-, and carbon fibres, and each type has distinct advantages and disadvantages. The fibrillar structure of aramid fibres gives them the ability to absorb considerable amounts of impact energy. Smallman and Ngan [10] show that impacting aramid fibres causes them to split into numerous microfibrils, which gives them a high resistance to the impact. The main properties of aramid fibre are high strength and low density, which result in a high specific strength. Aramid fibres exhibit a nonlinear, ductile behaviour under compression, as described by Chang [11]. UHMWPE fibre is a gel-spun multi-filament fibre produced from polyethylene. It exhibits high strength and high modulus with low weight, as well as being resistant to most chemicals. Marissen et al. [12] showed that UHMWPE fibres have a very high tensile strength but low compressive strength. However, the strain to fracture along the fibre direction is very large. This could make it desirable for use in composites under impact loading due to the enhanced damage tolerance. However, this should only be accomplished by hybridizing or using the fibre in combination with other fibres, such as carbon fibres, in order to achieve more desirable material properties and adequate stiffness. UHMWPE fibres show poor adhesion to matrix material systems used in composites due to their chemically inert polyolefin structure. Hence, surface treatments are needed in order to improve adhesion with the matrix material. Plasma treatment is an example of such a treatment.

The fibres in a composite significantly improve the mechanical properties of the composite, and as a result, they are the main contributing factor, when compared to the resin matrix, in improving the mechanical properties of the composite. Generally, fibres are designed to be loaded along their length and not across their width, and therefore, the orientation of the fibres creates highly direction-specific properties in the composite [13].

B. Composite Impact Testing

Impact on composites depends upon two primary variables, which are the geometry and material of the impacting bodies. Secondary variables include the mass of the bodies, drop height, and losses due to friction and other external factors. The performance of the materials undergoing impact comes down to the response of all the materials used. Talreja [14] describes fibre failure occurring at stresses exceeding the strength of the weakest fibre in the composite lamina. When this happens, the load transfers to the surrounding matrix's material regions. At the tip of the failed fibre, the shear stress concentrations cause damage to the matrix, causing localised debonding of the fibre from the matrix.

Matrix failure can be categorized into two distinct modes, matrix failure within a ply and matrix failure between plies. Matrix failure within a ply is known as interfibre fracture. It usually starts at the interface between the fibre and the matrix and propagates to the matrix. Harris [8] defines matrix failure between plies, also known as delamination, to be caused by interlaminar stresses.

The equations based on fibre failure are governed by longitudinal stresses in the fibre, whilst the equations based on matrix failure are governed by transverse and tangential stresses in relation to the fibre direction. The types of composite materials and their applications vary widely so that no single test can readily quantify the many potential impact situations and their subsequent effects. Hogg and Bibo [15] describe the impact 'resistance' of a composite to refer to the following:

- The ability of the composite to withstand a given impact force without any damage (resilience);
- The maximum force necessary to rupture or separate a composite structure, irrespective of prior damage (impact strength);
- The amount of energy that is absorbed by a given mass of the composite (crush resistance);
- The amount of damage that a composite can sustain during an impact without suffering undue reduction to a primary structural function after the impact occurs (damage tolerance).

Impact loading is usually taken to mean the impact of either an impactor or the composite itself at speeds in the range from 1 to 10 m/s. Impacts at lower speeds can still cause significant damage to composites if the momentum is large enough to induce matrix and fibre failure. Laminate composite plate impact tests usually comprise the impact of an impactor onto a plate-type specimen, shown schematically in Figure 3.

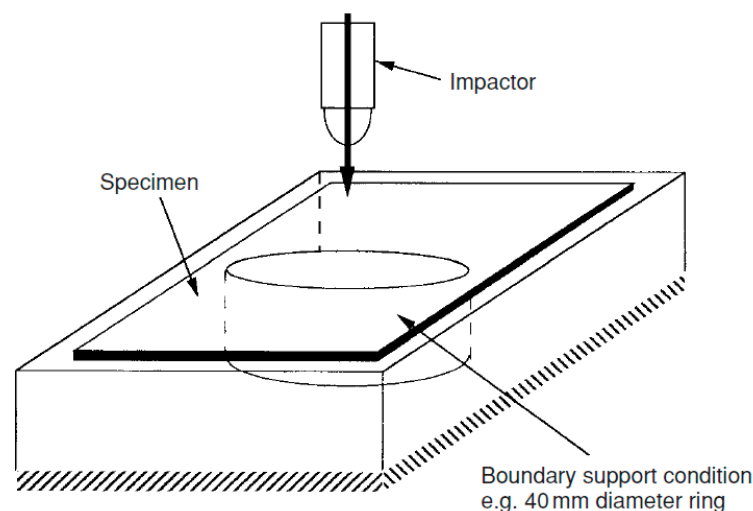


Figure 3. Typical laminate plate impact geometry [15].

This configuration is often used to assess the ultimate load resistance of the material and its energy-absorbing capabilities. Hogg and Bibo [15] show that it can be indicated that

the peak impact force is a result of the strain to failure of the reinforcing fibres, coupled with the initial stiffness of the composite plate, and is independent of resin chemistry.

C. Finite Element Analysis

The main aim of FEA (Finite Element Analysis) is to reduce the amount of experimentation and destructive testing needed in order to complete an analysis. One such FEA suite is 3DS Abaqus [16], which can either use the implicit modelling method based on static conditions or the explicit modelling method based on time and integration methods, as described by Roberts [17].

This explicit method is chosen in order to better understand the failure modes as well as to see how the failure propagates throughout the panel. Using the explicit method also allows the fibre failure to be modelled based on Hashin's failure criterion, which shows the regions where failure occurs. The Hashin failure criterion separates the failure of a composite by the tension and compression of the fibre and the tension and compression of the matrix, resulting in four equations which govern the failure of a composite; Roberts [17] and Hashin [18] define this.

The 3DS Abaqus [16] also contains damage evolution capability for fibre-reinforced materials [19]. This damage evolution uses a characterised progressive degradation of material stiffness, eventually leading to material failure. The damage evolution failure mode must be used in combination with Hashin's damage initiation criteria in order to best understand the propagation of damage.

2. Materials and Methods

In order to find a laminate that has the desired mechanical properties, an initial study was conducted using Autodesk Heliux Composite [20]. The software allows for the creation of laminates consisting of multiple layers of laminas. The base lamina was made up of a single layer of fabric surrounded by a resin matrix. The material properties from Table 2 were used in this case to create the lamina and, thereafter, laminates. Many factors have been taken into account at this stage, such as ease of handling, thickness, and fibre size. The most important factors were the availability of materials as well as cost. Therefore, the following fabrics with their corresponding GSM (Grams per Square Meter) weight were selected to be used based on their availability and cost:

1. 600 GSM Carbon Fibre;
2. 460 GSM Aramid Fibre;
3. 400 GSM Fibreglass;
4. 180 GSM UHMWPE.

The fibre direction of the laminates must be considered as well, as this is critical due to the anisotropic nature of the material. Hence, modelling is performed with the fibres in a $0/90^\circ$ orientation as well as in a $+45/-45^\circ$ orientation. Table 1 shows the chosen layups that have been used going forward. Layup 1 was used as a benchmark for the testing as it is currently used on the race vehicle. Layup 2 was chosen in order to provide a control for the testing as well as due to the low cost, which would allow for more test panels to be produced for a better sample size. Layup 3 was chosen due to its favourable thickness in relation to its density as well as having good mechanical properties. Layup 4 was chosen to investigate the effect of hybridizing using UHMWPE as well as due to the low density, which could aid in saving weight on the race vehicle.

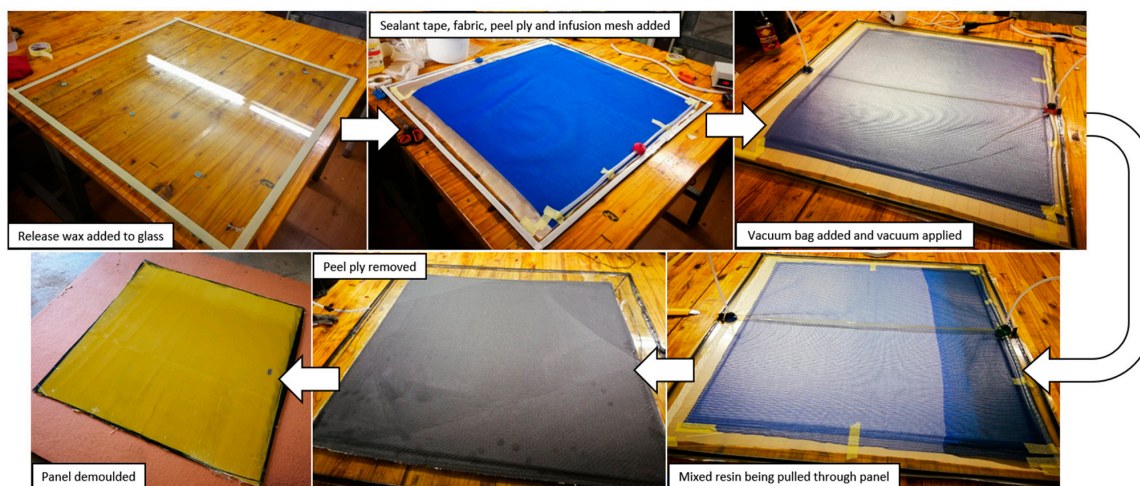
Table 1. Final layups for testing and analysis.

Ply	Layup 1	Layup 2	Layup 3	Layup 4
1	460 gsm Aramid	400 gsm Fibreglass	460 gsm Aramid	460 gsm Aramid
2	460 gsm Aramid	400 gsm Fibreglass	460 gsm Aramid	460 gsm Aramid
3	460 gsm Aramid	400 gsm Fibreglass	460 gsm Aramid	460 gsm Aramid
4	460 gsm Aramid	400 gsm Fibreglass	460 gsm Aramid	460 gsm Aramid
5	460 gsm Aramid	400 gsm Fibreglass	460 gsm Aramid	460 gsm Aramid
6	460 gsm Aramid	400 gsm Fibreglass	460 gsm Aramid	460 gsm Aramid
7	600 gsm Carbon	400 gsm Fibreglass	460 gsm Aramid	180 gsm Dyneema
8	600 gsm Carbon	400 gsm Fibreglass	460 gsm Aramid	180 gsm Dyneema
9	-	400 gsm Fibreglass	-	180 gsm Dyneema
10	-	400 gsm Fibreglass	-	180 gsm Dyneema
11	-	-	-	180 gsm Dyneema

In total, the following panels were manufactured using the method outlined below:

- 3x Layup 1, 0/90°;
- 1x Layup 1, -45/+45°;
- 6x Layup 2, 0/90°;
- 1x Layup 2, -45/+45°;
- 2x Layup 3, 0/90°;
- 1x Layup 3, -45/+45°;
- 2x Layup 4, 0/90°;
- 1x Layup 4, -45/+45°.

The test samples were manufactured at the University of Johannesburg's Auckland Park campus in the composites laboratory. The method used to manufacture the panels was resin infusion, chosen in order to maintain the consistency between all the test samples. Figure 4 shows the steps taken to manufacture the test panels.

**Figure 4.** Manufacturing of test sample.

Once all these steps have been completed, the panel needs to undergo a post-curing process, as described by the manufacturer of the epoxy resin (Gurit Prime 27 LV). This is vital to ensure the achievement of the correct mechanical properties of the resin. Once the post-cure at 50 °C for 16 h is complete, the test sample can be trimmed, and the holes cut. It was decided to manufacture a minimum of two panels in the 0/90° fibre orientation and

one in the $+45/-45^\circ$ fibre orientation. This was chosen due to the higher cost involved in manufacturing panels with fibres in the $+45/-45^\circ$ orientation.

3. Modelling and Test Sample Design

The initial point of consideration is into the modelling of the laminate test panel to gain a better understanding of the effect of different layup configurations. Constraints for the modelling are based on the race vehicle in terms of the mounting method, laminate thickness allowance, and span area. The guard is limited in thickness due to the close proximity of the engine to the guard, as well as the aspect of ground clearance that needs to be maximised. The laminate thickness is, therefore, limited to 6 mm.

The size of the laminate panel is determined from the largest unsupported area of the belly guard. This gives a worst-case scenario as the larger the unsupported area, the more the laminate is allowed to deform and cause potential damage and failure. From measurements taken from the existing belly guard, as shown in Figure 5, the largest unsupported area is area 2, under the engine, which equates to a total area of 0.43 m^2 . Hence, the square panel needs to have a maximum unsupported length of 0.655 m on each side. For simplicity, this is rounded off to 0.65 m. Some assumptions need to be made in order to determine a loading case and restrictions for the modelling software. For this analysis, 3DS Abaqus [16] was used to determine the laminate strength from explicit, dynamic conditions. In order to determine the material properties used in the analysis, datasheets, the literature, and software programs are used. Material data are entered into Autodesk Heliuss Composite[®] 2017 [20] software to determine the laminate properties. The values for the bare fibre yarns are entered into the software to determine the material properties of a fabric in conjunction with a resin matrix. From these properties, a lamina is simulated in Autodesk Heliuss Composite [20] with fibres in the $0^\circ/90^\circ$ direction in order to determine the properties of a woven fabric encased in a matrix. Table 2 gives the material properties obtained to be used in the Finite Element Analysis (FEA) [21–25].

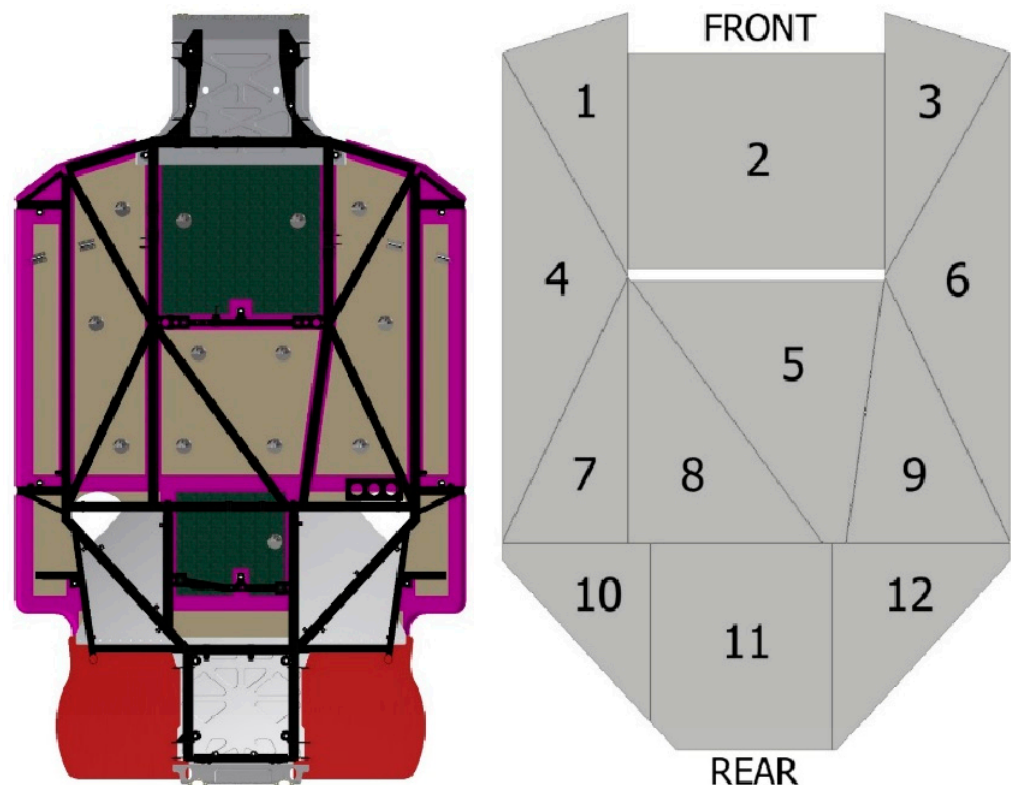


Figure 5. Underside protection area.

Table 2. Material Properties to be used in FE analysis [21–25].

Property	Unit	Fibreglass	Aramid	Carbon	UHMWPE
Elastic modulus (E_{11})	GPa	72.4	124	225	116
Elastic modulus (E_{22})	GPa	72.4	124	225	116
Elastic modulus (E_{33})	GPa	9	5	15	3
Poisson’s ratio (ν_{12})	-	0.13	0.24	0.05	0.20
Poisson’s ratio (ν_{13})	-	0.25	0.35	0.21	0.20
Poisson’s ratio (ν_{23})	-	0.25	0.35	0.21	0.20
Shear Modulus (G_{12})	GPa	4.8	1.4	7.0	0.5
Shear Modulus (G_{13})	GPa	5.6	2.6	15.0	3.3
Shear Modulus (G_{23})	GPa	5.6	2.6	15.0	3.3
Density (ρ)	kg/m ³	2600	1440	1800	970
Longitudinal Tensile Strength (X_T)	MPa	863.4	1011	917.4	1075
Longitudinal Compressive Strength (X_C)	MPa	780.6	228.6	494.5	268.8
Transverse Tensile Strength (Y_T)	MPa	863.4	1011	917.4	1075
Transverse Compressive Strength (Y_C)	MPa	780.6	228.6	494.5	268.8
Longitudinal Shear Strength (S_{12})	MPa	109.4	39.86	82.31	45.1
Transverse Shear Strength (S_{23})	MPa	109.4	39.86	82.31	45.1
Longitudinal Tensile Fracture Energy (G_{XT})	J	27,170	146,210	112,700	168,430
Longitudinal Compressive Fracture Energy (G_{XC})	J	24,150	9840	25,900	10,350
Transverse Tensile Fracture Energy (G_{YT})	J	930	230	500	280
Transverse Compressive Fracture Energy (G_{YC})	J	930	230	500	280

In order to best represent the impact that could occur on the belly guard from a rock, an approximation needs to be made to best represent an average rock that would be encountered on a racing stage. The size of the impactor is based on the average rock size that causes damage on a racing stage and can be seen in Figure 6, where the height is 225 mm and the diameter before the spacer is 150 mm.

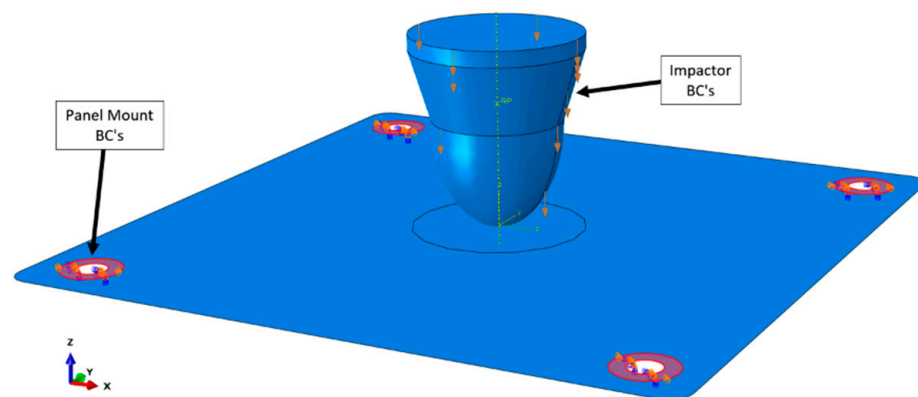


Figure 6. Laminate Boundary Conditions.

The composite plate needs to be given constraints and fixtures in order to carry out the FEA.

The boundary conditions are as follows:

- Panel Mount: Figure 6 shows the laminate boundary conditions. The highlighted areas in Figure 6 can be assumed to have no transverse movement in the Z direction due to the clamping action of the retaining plate flange against the laminate panel. The diameter of the clamping area is 70 mm. For simplicity, it is also assumed that there is no movement allowed in the mounting holes themselves;
- Impactor: The impactor is constrained to move in the Z direction only with no rotation permissible. It impacts the plate perpendicularly at the centre.

The loads applied to the panel in the simulations have to be equal to the test loads. This is required to draw a proper comparison between the simulated and test results. In order to determine the applied load to the panel, a mass and height evaluation is performed. In addition, the velocity results of the experimental testing are used. This gives an impact velocity of 6.5 m/s and an impactor mass of 172.6 kg. These values are entered into 3DS Abaqus [16] as the loads for the impactor.

A. Modelling Parameters and Mesh

In order to perform the FEA analysis, an element type as well as a base feature shape needs to be chosen. In this case, the panel is modelled as a shell using linear quadrilateral elements of type S4R as well as linear triangular elements of type S3R. This is chosen as it allows for a faster run time whilst still allowing for the necessary failure criterion to be applied in the analysis. When a shell-type base feature is used, the composite layers in the laminate can be assigned to the shell. This gives the shell the properties of the composite laminate and allows for the correct material properties to be assigned to the shell.

Seeing that the type of modelling used is explicit, a time step needs to be determined for the analysis. Taking the speed of the impactor before impact as 6.5 m/s, as well as the maximum travel distance allowed by the impactor before it makes contact with the mounting base of 205 mm, an ideal step time can be determined. Considering a case where no test panel is fitted and using the above values, a travel time of 0.031538 s is calculated. This means that unhindered, the impactor will take 0.031538 s to cover the distance from where the test panel would be to the base of the mounting jig. So, in order to make sure that the analysis is completed so that all the necessary data are calculated and captured, a time greater than 0.031538 is necessary. Therefore, a time step of 0.035 s is used.

To determine the correct mesh element size to use, a sensitivity analysis needs to be performed. This ensures that values are obtained that can be trusted while also allowing for the fastest analysis run time possible. Using too large a time step for this case could cause an instance where the loading causes material failure, and the results would be inconsistent. This is due to the element deletion that the software uses when an element has exceeded the maximum allowed stress.

The deletion of the elements would cause inconsistencies when different mesh element sizes are used. Therefore, a time step of 0.002 s is used for the mesh sensitivity analysis to ensure that this does not occur. A global mesh size of 30 mm is chosen and fixed throughout all the analyses. The centre impact circle element size, where the maximum stress occurs, is then varied to determine the convergence.

From the results, good convergence with a relatively large element size is observed. Nonetheless, an optimised mesh is used in order to provide accurate results with minimal run time. The global mesh size used is 15 mm, with a more refined mesh size of 6 mm used in the centre and mounting locations, as seen in Figure 7. The global mesh size, in this case, refers to all element sections of the plate except the centre and mounting hole locations.

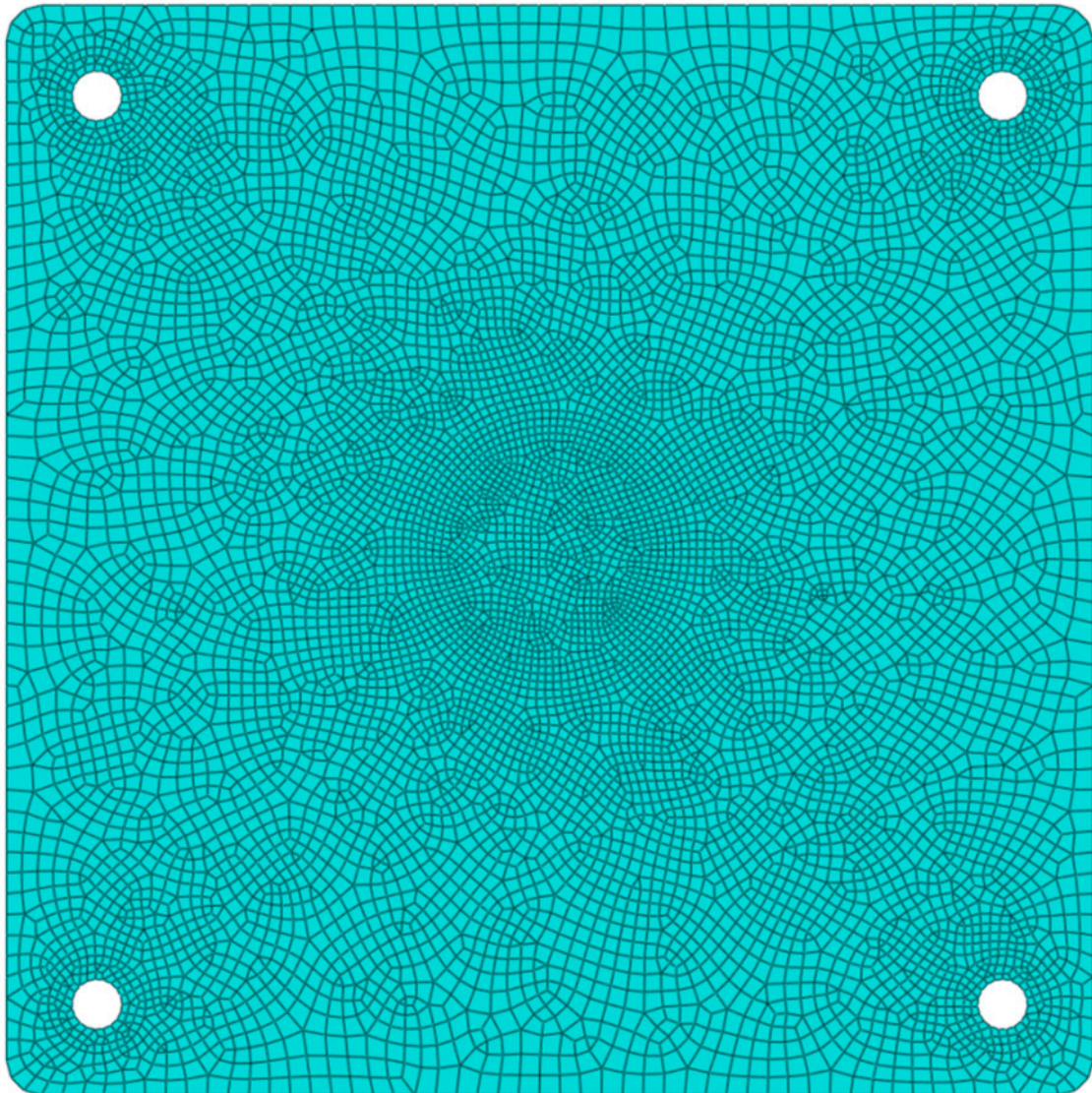


Figure 7. Test plate mesh.

Using this mesh with the same loading case and time step as used for the convergence, we obtain the results in Table 3. From this, it can be seen that the optimised mesh has a maximum stress very close to that of the maximum mesh, with a significantly shorter time taken to complete the analysis. The computer used has the following specifications: Intel Core i7 7700k CPU; 16 GB DDR4 RAM; and Nvidia GTX1080Ti GPU.

Table 3. Optimised mesh results.

	Maximum	Optimised
Element size global (mm)	30	15
Element size centre (mm)	1	6
No of Nodes	37,359	8683
No of Elements	37,965	8697
Max stress (MPa)	5.617×10^8	5.263×10^8
Time taken (HH:MM:SS)	01:02:02	00:02:18

The mesh size for the impactor is chosen to be 5mm, as this is not as critical as the panel. The stiffness of the steel impactor is much greater than that of the test panels. Therefore, the impactor is modelled as a rigid body.

B. Modelling Results

An analysis of each panel layup is performed with fibres in the 0/90° orientation as well as in the +45/−45° orientation in relation to the coordinate system in 3DS Abaqus [16], as seen in Figure 6. Hashin’s failure criteria, as well as damage evolution, are chosen to be used in the analysis. This gives the best estimation of progressive fibre and matrix failure. A breakdown of the results of each analysis is given in Table 4.

The results obtained show a significant difference between the 0/90° and +45/−45° fibre orientations for each panel layup. This is due to the +45/−45° fibres being in line with the diagonally opposing mounting point. The displacement at which failure occurs for each orientation tends to be lower for the +45/−45° orientation. This is due to a smaller number of fibres and matrix material having to withstand the load compared to the 0/90° direction. The 0/90° fibre orientation tends to distribute the load more evenly; however, high loads do still tend to show at the mounting hole locations. Generally, the first fibre tensile failure occurs in the centre where the impactor makes contact, while the first fibre compressive failure occurs at the mounting holes.

Table 4. Modelling results.

Layup Number		1		2		3		4	
Fibre Orientation		0/90°	45/135°	0/90°	45/135°	0/90°	45/135°	0/90°	45/135°
Displacement (mm)		39.87	39.22	39.24	39.88	40.07	39.35	40.3	39.5
Max. von Mises Stress (MPa)		797.3	1202	786.4	1139	824.6	1101	996.1	1249
Maximum Impactor Displacement (mm)		150.5	98.3	159.6	153.9	149.7	93.29	128.7	61.1
Hashin	Displacement at Tensile First Fibre Failure	13.05	13.01	41.54	25.88	28.96	24.35	29.24	26.83
	Displacement at Compressive First Fibre Failure	26.57	17.5	34.78	30.43	24.46	15.41	24.77	15.69
	Displacement at Tensile First Matrix Failure	26.57	13.01	41.54	19.11	28.96	24.35	27.01	26.83
	Displacement at Compressive First Matrix Failure	26.57	17.5	34.78	30.43	24.46	15.41	22.5	15.69
Damage Evolution	Displacement at Tensile First Fibre Failure	48.53	32.91	46.09	25.88	57.24	37.29	65.41	39.5
	Displacement at Compressive First Fibre Failure	56.86	32.91	41.54	37.56	59.29	30.92	57.39	33.3
	Displacement at Tensile First Matrix Failure	31.01	19.74	32.56	25.88	33.42	28.75	33.67	31.16
	Displacement at Compressive First Matrix Failure	31.01	24.2	41.54	35.09	31.19	22.13	29.24	22.41

Figure 8 shows the deceleration of the impactor when contact is made with the laminate. This is calculated from the resultant velocity output of the impactor during impact from each model.

The higher the deceleration of the impactor, the more the laminate resists the impact force; hence, deductions about the most suitable laminate can be made. Layup 4 has very desirable properties due to the use of UHMWPE, which is more resistant to impact. This can be seen in the higher deceleration of the impactor compared to the other laminate layups. The lower maximum displacement in comparison to the other laminate panels, as seen in Table 4, also indicates a higher out-of-plane strength, which is the desired property for this investigation. Layup 2 has expected degradation values due to the high strength but low ductility and fracture energies of the fibreglass material. The deceleration is more gradual due to the high compression strength of the fibres. The fibre orientation has less of an effect on the results in comparison to other laminate sets. This is due to the low ductility and out-of-plane strength. Layup 3 has more impact resistance than the currently used layup 1, which can be seen from the maximum displacement values and stresses. Hence, the use of carbon fibre in laminates that undergo impact loadings is not recommended for this case. It must be noted that there is no direct correlation between the von Mises stress and the displacement of the panel under load. This is due to the difference in elastic moduli between the various fibres used for the analysis. The higher modulus fibres have less deflection under load due to their higher in-plane strength.

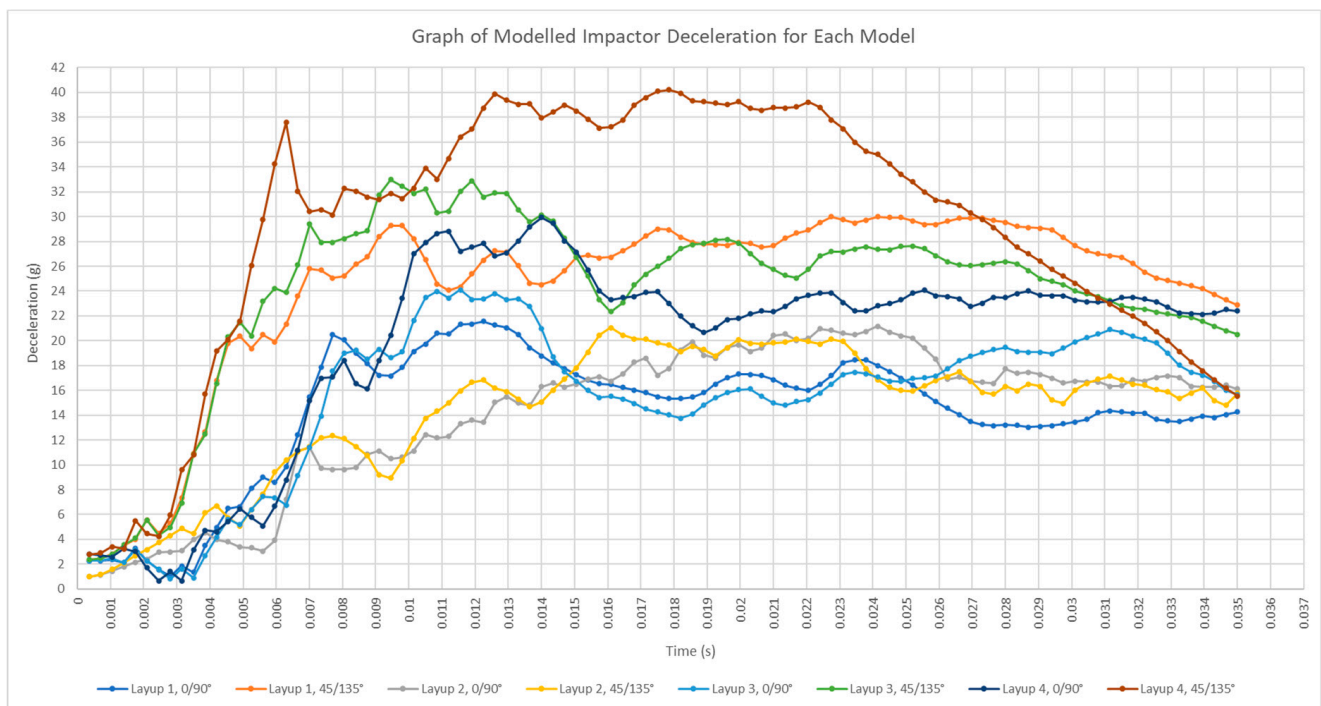


Figure 8. Graph of impactor deceleration for all tests.

C. Stress Concentrations

Figure 9 shows the modelled stress concentrations for layups from 1 to 4. The fibres in the 0/90° orientation show a more distributed region of stress with concentrations around the mounting holes. This is to be expected due to the hole locations in the panel having to take most of the tensile load in the corner regions. Layup 2, which utilizes only glass fibres, has a more distributed stress when comparing the hole locations to the impactor impact zone. This is due to the high stiffness and low ductility of the fibres. Layups 1, 3, and 4 contain Aramid fibres, which have high in-plane strength. This is evident from the higher stress concentration in the impact zone compared to those of the mounting hole locations.

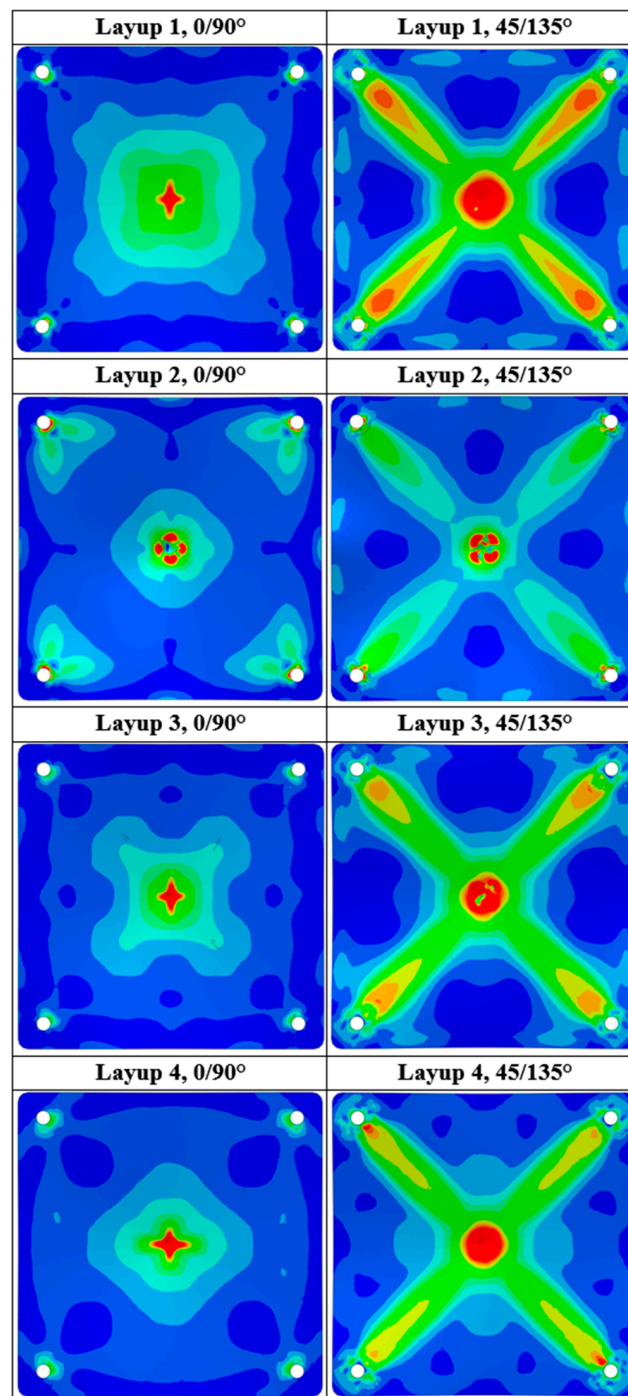


Figure 9. Modelled panel stress concentrations.

4. Experimental Testing

The main experimental apparatus is the drop tester at the University of Johannesburg's Auckland Park campus. The drop tester forms the main part of the apparatus that is used to conduct the testing. The combined drop sled and impactor mass was 172.6 kg, and the drop height was 2.952 m in order to match the impact force that occurred on a vehicle belly guard. In order to hold the test sample in place during the testing, a sample-holding jig needs to be designed and manufactured. Using the previous test sample constraints as well as the test sample fixtures, the design can be carried out. The designed jig is shown in Figure 10. The mounting height is taken to be 200 mm, which is considered sufficient to ensure that no impactor or drop tester damage can occur. All the parts are manufactured

from mild steel except the horizontal tubes, which are made of 4130 steel as per the race vehicle. In order to determine the position of the drop tester during the test, sensors are needed at predetermined positions to sense the time and position of the drop test cart as it comes past.

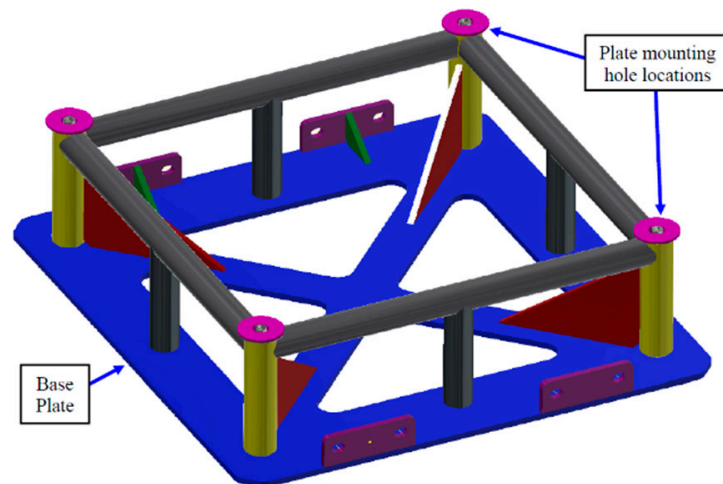


Figure 10. Test sample mounting jig.

Skye-e P1C1B1204NS4A2 inductive proximity switches are used in this case to provide the sensing. To calculate the acceleration and velocity of the drop test cart, a pair of sensors is placed at the top of the drop tester where the cart is released from, and another pair is placed at the bottom right before contact with the test sample.

Four accelerometers are also used to record the impact of the drop sled on the laminate panels. Two 16G sensors (Analog Devices ADXL326) and two 200G (Analog Devices ADXL377) sensors are used for redundancy. These can be seen in Figure 11.



Figure 11. Accelerometer mounting.

In order to further record and capture the test results, a high-speed camera and printed scale are used to verify all results, as seen in Figure 12. A Sony Cyber-shot DSC-RX10 IV camera is used to capture video footage at 1000 frames per second, which is recorded and saved after each drop test.

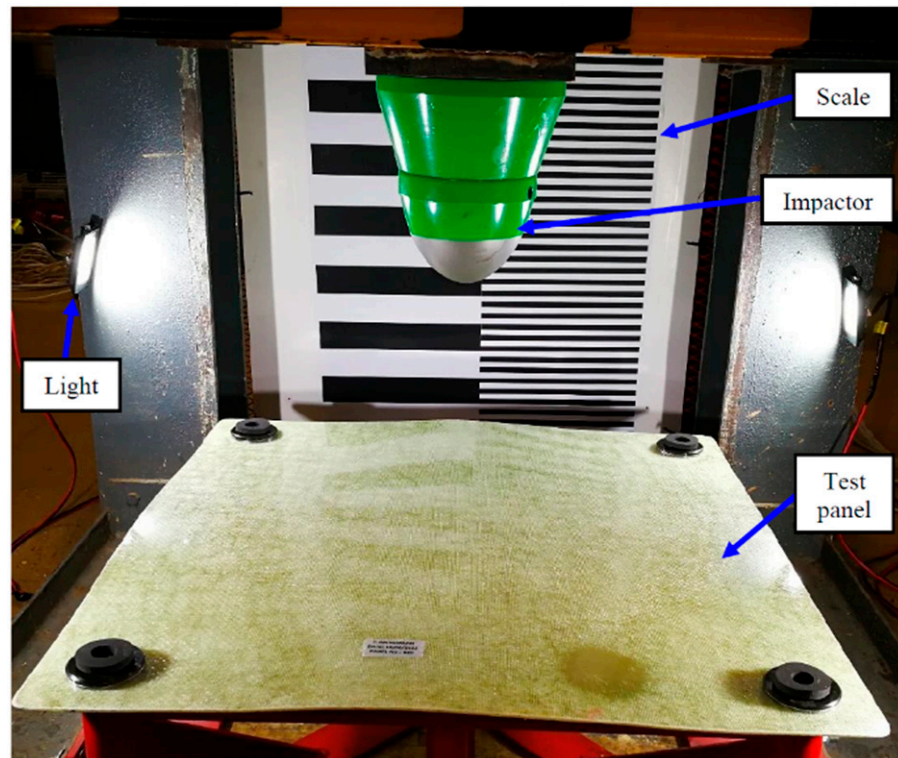


Figure 12. Test setup.

5. Results and Discussion

A. Sled Velocity

In order to verify the sled velocity, a comparison is performed between the velocity obtained using the proximity sensors and the velocity obtained from the high-speed camera. Table 5 shows the values obtained from each method, and it can be seen that there is a good correlation between the results. The difference between the data sets is due to friction and other external factors affecting the motion of the drop sled. The velocity obtained from the proximity sensors assumes that the sled is under free fall conditions due to gravity with no friction, hence the higher velocity values. From the correlation between the data, it can be deduced that the results from the high-speed camera are accurate and can be used for the analysis and for the drawing of conclusions.

Table 5. Velocity result comparison.

Panel	1A	1B	1C	1D	2C	2D	2E	2F	2G	3A	3B	3C	4A	4B	4C
Drop Test No.	1	2	3	4	5	6	7	8	9	10	11	12	13	14	15
Velocity from Proximity Sensors (m/s)	7.322	7.312	7.351	7.645	7.390	7.273	7.449	7.361	7.380	7.341	7.341	7.586	7.380	7.478	7.390
Velocity from High Speed Camera (m/s)	6.539	6.507	6.352	6.625			6.176	6.352	6.454	6.438	6.578	6.625	6.460	6.479	6.539
Difference	0.782	0.805	0.999	1.020			1.273	1.009	0.927	0.903	0.764	0.961	0.921	1.000	0.851

B. Accelerometer Results

The maximum accelerometer values that were recorded during the drop testing impact can be seen in Figure 13. From the results, it can be seen that there is a good correlation

between the 16 g sensors and the 200 g sensors. It must be noted that for values above 16 g, only the results obtained from the 200 g sensors can be used. Panels 3 and 4 have a higher maximum impactor deceleration and, hence, a higher impact resistance.

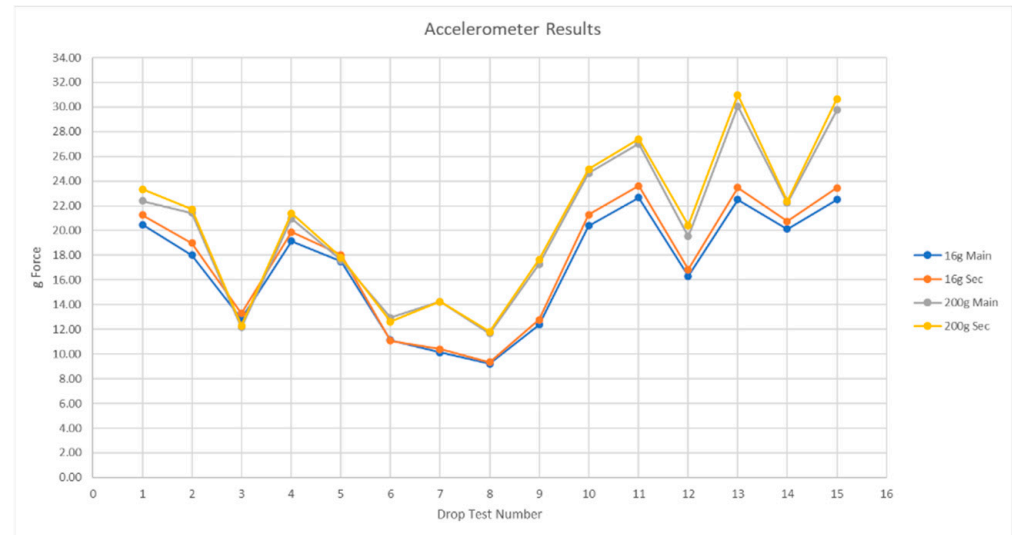


Figure 13. Graph of accelerometer results.

C. Impact Results

Figures 14–19 show some of the results of the impact damage to the panels. Panel 1 ($0^\circ/90^\circ$) underwent total failure at two of the mounting holes. The discrepancies in the failure location can be attributed to the impact not occurring exactly in the centre of the panel. This caused a higher stress concentration on the mounting holes on one side of the panel, resulting in premature failure. The results are in agreement with the stress concentrations seen in Figure 8.



Figure 14. Panel 1 ($0^\circ/90^\circ$).

Panel 1 ($+45^\circ/-45^\circ$) shows that total ply failure occurred through the mounting holes on one side. This, again, could be due to misalignment of the impactor, causing impact to occur off-centre. The matrix cracking can be seen propagating from the impact point to the mounting hole locations. This was correctly predicted by the model (see Figure 8).



Figure 15. Panel 1 (+45°/−45°).



Figure 16. Panel 3 (0°/90°).



Figure 17. Panel 3 (+45°/−45°).



Figure 18. Panel 4 ($0^\circ/90^\circ$).



Figure 19. Panel 4 ($+45^\circ/-45^\circ$).

Panel 3 ($0^\circ/90^\circ$) again shows signs of a possible off-centre impact due to failure occurring at two of the mounting hole locations. This is similar to the result obtained from panel 1 ($0^\circ/90^\circ$), indicating that some of the panels are undergoing the same off-centre impact.

Panel 3 ($+45^\circ/-45^\circ$) shows that the failure that occurred was limited to a single mounting hole location. The direction and location of the matrix cracking were also predicted by the model. However, the premature failure at one location did not allow for any more propagation of the load to occur. The failure at one corner can be attributed to a different batch of material being provided by the supplier, which could have differing material properties from what is expected. Fibre failure and matrix cracking still occurred along the directions between opposite mounting holes, as expected from the modelling data, but not to the extent expected.

Panel 4 ($0^\circ/90^\circ$) shows that the failure region was also predicted by the model. The indentation made by the impactor and the lack of significant damage at the mounting hole locations indicate a panel that has a high out-of-plane strength. The failure along the fibre direction in the centre of the panel is also predicted by the model. The consistency of the matrix cracking and lack of localized damage at only certain mounting hole locations indicate that the impact occurred in the centre of the panel.

It can be seen that fibre ply delamination has occurred between the UHMWPE fibre layers and the aramid fibres. This amount of delamination is more prevalent than in the other tested panels. This is due to the lower fibre wettability of UHMWPE. The larger strain to fracture property of the material along the fibre direction is also a contributing factor to the cause of delamination.

Panel 4 (+45°/−45°) shows that the panel encountered total failure at two of the mounting holes. This, again, can be attributed to an off-centre impact. The regions of matrix cracking between opposing mounting hole locations were also predicted by the model. The failure of the panel around two of the mounting hole locations would cause the load not to be distributed evenly during the test. Less delamination occurred from this test compared to the tests of panel 4 (0°/90°). This can be attributed to the load being distributed along the length of the fibres, causing less out-of-plane strains.

D. Accelerometer Results Comparison

Figure 20 shows the results obtained from the accelerometer for all the drop tests. From this graph, the following can be deduced:

- Panel 2 shows the least impact resistance but good repeatability, which is as expected. Therefore, this layout is a good control to be used as a reference going forward;
- Panels 3 and 4 show very good repeatability during the initial impact phase. However, they deviate afterwards due to various aspects such as off-centre loading and possible material differences;
- The use of carbon fibres does not improve the impact resistance of the panel;
- The +45/−45° fibre orientation panels perform better than the 0/90° fibre-orientated panels;
- The use of UHMWPE fibres improves the impact resistance of the panel significantly whilst also reducing the overall weight.

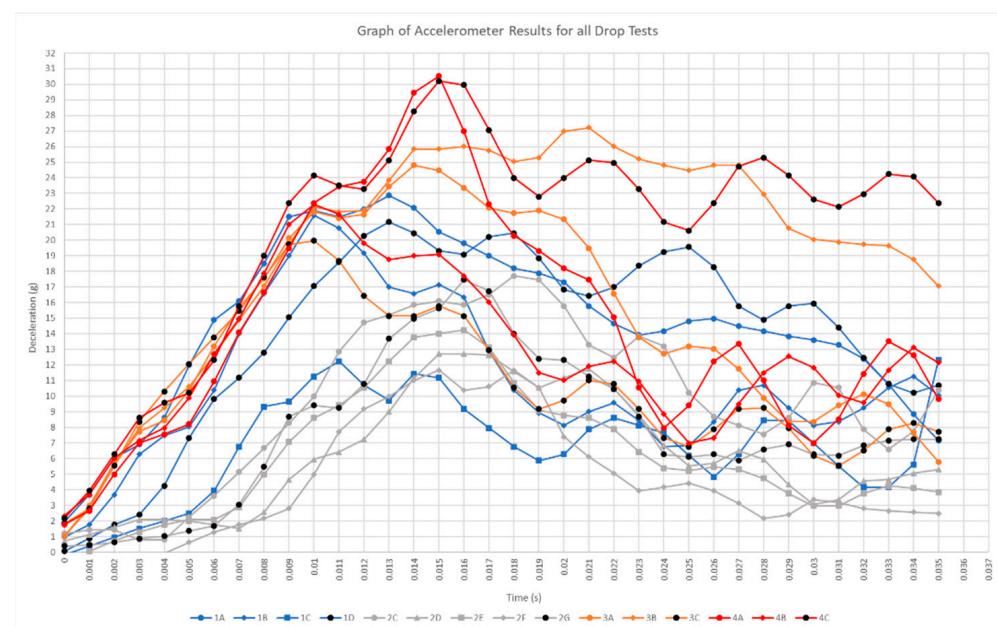


Figure 20. Accelerometer results for all drop tests.

Using aramid fibres is a good compromise between impact resistance, weight, and cost. Panels that used aramid fibres also exhibited good repeatability and minimal delamination. UHMWPE fibres significantly increase the impact resistance of the panel; however, there are some drawbacks. Dyneema is costly, and the high strain to failure rate causes delamination when hybridised with other fibre materials.

6. Conclusions and Recommendations

Many layups were analysed in order to find the best ones suitable to the applicable problem. From the initial analysis, four laminate layups were proposed for further analysis and experimental testing. An explicit analysis was performed using 3DS Abaqus [16] FEA software with the appropriate mesh and boundary conditions. The impactor deceleration was modelled, which was the main parameter used in order to compare the modelling data to the experimental data. Hashin and damage evolution criteria were used to predict fibre and matrix failure for the laminate panels.

Experimental testing was carried out using a drop tester. An impactor was designed that was representative of the shape of rocks that could come into contact with the belly guard. The combined drop sled and impactor mass was 172.6 kg, and the drop height was 2.952 m. A laminate test panel was designed that had attributed to the current race car in terms of the largest unsupported area, thereby simulating damage in the worst case. A corresponding frame was designed that had attachments to the laminate panel that mimicked the type used on the race car, thereby ensuring representative load cases.

Seventeen test panels of various layups and fibre orientations were manufactured and drop-tested using sensors and data loggers to capture data during the tests. Some discrepancies were experienced during the testing phase as some of the panels encountered off-centre impact loadings, which caused premature failure of the laminate panels in concentrated areas.

Comparing the data obtained from the modelling and experimental testing, the following can be concluded:

- The stress distribution obtained from the modelled data agreed with the experimental data in terms of the location of the matrix and fibre failure;
- The modelled and experimental impactor deceleration show good agreement in the initial loading phase up to the maximum deceleration;
- The modelled impactor data did not accurately predict the failure mechanisms after the maximum initial impact loading had occurred;
- The Hashin and damage evolution criteria showed some of the expected results in terms of fibre and matrix failure. However, some deviation from the experimental results was found;
- The use of carbon fibres for low-speed impact on composite panels is not recommended as it does not increase impact resistance;
- Simply using more aramid material increased the impact resistance of the laminate panels;
- The use of UHMWPE fibres greatly increased the impact resistance of the laminate panels. However, delamination occurred more easily between the UHMWPE fibres and fibres of other materials in the laminate. This is, however, not of great significance as only a singular impact is being considered without the case of another impact in the same zone.

Author Contributions: Conceptualization, T.B. and C.R.B.; methodology, T.B. and C.R.B.; software, T.B.; validation, T.B. and C.R.B.; formal analysis, T.B.; investigation, T.B.; resources, T.B.; data curation, T.B.; writing—original draft preparation, T.B.; writing—review and editing, T.B. and C.R.B.; visualization, T.B. and C.R.B.; supervision, C.R.B.; project administration, T.B. and C.R.B.; funding acquisition, T.B. All authors have read and agreed to the published version of the manuscript.

Funding: This research received no external funding.

Data Availability Statement: The data presented in this study are available on request from the corresponding author. The data are not publicly available due to intellectual property restrictions.

Conflicts of Interest: The authors declare no conflict of interest.

References

1. Aymerich, F.; Pani, C.; Priolo, P. Damage response of stitched cross-ply laminates under impact loadings. *Eng. Fract. Mech. Eng. Fract. Mech.* **2007**, *74*, 500–514. [CrossRef]
2. Aymerich, F.; Pani, C.; Priolo, P. Effect of stitching on the low-velocity impact response of [03/903]s graphite/epoxy laminates. *Compos. Part A* **2007**, *38*, 1174–1182. [CrossRef]
3. Indermuehle, K.; Barnes, G.; Nixon, S.; Schrank, M. Simulating Composites Crush and Crash. In Proceedings of the 50th AIAA/ASME/ASCE/AHS/ASC Structures, Structural Dynamics, and Materials Conference, Palm Springs, CA, USA, 4–7 May 2009.
4. Bouwmeester, J.G.H.; Marissen, R.; Bergsma, O.K. Carbon/Dyneema® Intralaminar Hybrids: New Strategy to Increase Impact Resistance or Decrease Mass of Carbon Fiber Composites. In Proceedings of the 26th International Congress of the Aeronautical Sciences, Anchorage, AK, USA, 14–19 September 2008.
5. Attwood, J.P.; Khaderi, S.N.; Karthikeyan, K.; Fleck, N.A.; Wadley, H.N.G.; Deshpande, V.S. The out-of-plane compressive response of Dyneema composites. *J. Mech. Phys. Solids* **2014**, *70*, 200–226. [CrossRef]
6. Abrate, S. Modeling of impacts on composite structures. *Compos. Struct.* **2001**, *51*, 129–138. [CrossRef]
7. Balasubramanian, M. *Composite Materials and Processing*; CRC Press: Boca Raton, FL, USA, 2014.
8. Harris, B. *Engineering Composite Materials*; The Institute of Materials: London, UK, 1999.
9. Campbell, F. *Structural Composite Materials*; ASM International: Park, OH, USA, 2010.
10. Smallman, R.; Ngan, A. Non-metals II—Polymers, plastics, composites. In *Physical Metallurgy and Advanced Materials*; Elsevier: Amsterdam, The Netherlands, 2007; pp. 549–581.
11. Chang, K.K. *Aramid Fibres*; Du Pont de Nemours: Wilmington, DE, USA, 2012.
12. Marissen, R.; Smit, L.; Snijder, C. Dyneema Fibers in Composites, the Addition of Special Mechanical Functionalities. In Proceedings of the Advancing with Composites 2005, International Meeting on Composite Materials, Naples, Italy, 11–14 October 2005; pp. 1–12.
13. Gurit. Guide to Composites. January 2013. Available online: <http://www.gurit.com/files/documents/guide-to-compositesv5webpdf.pdf> (accessed on 2 March 2014).
14. Talreja, R. Fatigue of Composite Materials: Damage Mechanisms and Fatigue-Life Diagrams. *Proc. R. Soc. Lond.* **1981**, *378*, 461–475.
15. Hogg, P.J.; Bibo, G.A. Impact and Damage Tolerance. In *Mechanical Testing of Advanced Fibre Composites*; Woodhead Publishing Limited: Cambridge, UK, 2000; p. 378.
16. *Dassault Systemes*; ABAQUS Inc.: Johnston, RI, USA, 2022.
17. Roberts, R. *Modeling Hybrid Composites using Tsai-Wu and Hashin Failure Criterion*; Aerospace Engineering Commons: Columbus, OH, USA, 2020.
18. Hashin, Z. Failure Criteria for Unidirectional Fiber Composites. *J. Appl. Mech.* **1981**, *58*, 846–852. [CrossRef]
19. Simulia. 23.3.3 Damage Evolution and Element Removal for Fiber-Reinforced Composites. 2011. Available online: <http://130.149.89.49:2080/v6.11/books/usb/default.htm?startat=pt05ch23s03abm45.html> (accessed on 5 September 2022).
20. Autodesk. *Heliux Composite*; Autodesk: San Francisco, CA, USA, 2016.
21. Performance Composites. Mechanical Properties of Carbon Fibre Composite Materials, Fibre/Epoxy resin (120 °C Cure). July 2009. Available online: http://www.performance-composites.com/carbonfibre/mechanicalproperties_2.asp (accessed on 11 November 2019).
22. Texas Tech University. Material Selection. 1996. Available online: <http://www.tsgc.utexas.edu/tadp/1996/reports/tech/material2.html> (accessed on 11 November 2019).
23. Performance Composites. Fiberglass and Composite Material Design Guide. Available online: <http://www.performancecomposites.com/about-composites-technical-info/122-designing-with-fiberglass.html> (accessed on 5 November 2019).
24. Johnson, R.R.; Kural, M.H.; Mackey, G.B. *Thermal Expansion Properties of Composite Materials*; National Aeronautics and Space Administration (NASA): Hampton, VA, USA, 1981.
25. Eurofibers. Dyneema® Fact Sheets. April 2012. Available online: <https://issuu.com/eurofibers/docs/name8f0d44/2> (accessed on 25 November 2019).

Disclaimer/Publisher’s Note: The statements, opinions and data contained in all publications are solely those of the individual author(s) and contributor(s) and not of MDPI and/or the editor(s). MDPI and/or the editor(s) disclaim responsibility for any injury to people or property resulting from any ideas, methods, instructions or products referred to in the content.